Earth and Planetary Science Letters 440 (2016) 92–104

Contents lists available at ScienceDirect

Earth and Planetary Science Letters

www.elsevier.com/locate/epsl

The role of crustal and eruptive processes versus source variations in controlling the oxidation state of iron in Central Andean magmas

Stephanie B. Grocke [a,b,*], Elizabeth Cottrell [a], Shanaka de Silva [b], Katherine A. Kelley [c]

[a] Smithsonian Institution, National Museum of Natural History, Washington, DC 20560, USA
[b] College of Earth, Ocean and Atmospheric Sciences, Oregon State University, Corvallis, OR 97331, USA
[c] Graduate School of Oceanography, University of Rhode Island, Narragansett, RI 20882, USA

ARTICLE INFO

Article history:
Received 8 July 2015
Received in revised form 21 January 2016
Accepted 24 January 2016
Available online xxxx
Editor: T.A. Mather

Keywords:
Central Andean volcanic zone
crustal assimilation
oxygen fugacity
subduction
wet chemistry

ABSTRACT

The composition of the continental crust is closely tied to subduction zone magmatism. Elevated oxygen fugacity (fO_2) plays a central role in fostering crystallization of oxide minerals and thereby aids in generating the calc-alkaline trend of iron depletion that characterizes the continents. Along continental margins, arc magmas erupt through continental crust and often undergo extensive differentiation that may modify magmatic fO_2. The importance of the subducting slab and mantle wedge relative to the effects of this differentiation on the fO_2 recorded by continental arc magmas remains relatively unconstrained. Here, we focus on the effect of differentiation on magmatic fO_2 using a suite of 14 samples from the Central Volcanic Zone (CVZ) of the Andes where the continental crust is atypically thick (60–80 km). The samples range in composition from ~55 to 74 wt% SiO_2 and represent the Neogene history of the arc. Samples are basaltic andesite to rhyolite and span a range of radiogenic isotopic compositions ($^{87}Sr/^{86}Sr$ = ~0.705–0.712) that represent 30 to 100% crustal assimilation. We use several proxies to estimate the fO_2 recorded by lavas, pumice, and scoria: (1) whole rock $Fe^{3+}/\Sigma Fe$ ratios, (2) $Fe^{3+}/\Sigma Fe$ ratios in quartz-hosted melt inclusions, and (3) Fe–Ti oxide oxygen-barometry. Comparison of the fO_2 calculated from bulk $Fe^{3+}/\Sigma Fe$ ratios (post-eruptive) with that derived from Fe–Ti oxides or melt inclusion $Fe^{3+}/\Sigma Fe$ ratios (pre-eruptive), enables us to quantify the effect of syn- or post-eruptive alteration, and to select rocks for bulk analysis appropriate for the determination of pre-eruptive magmatic fO_2 using a strict criterion developed here.

Across our sample suite, and in context with samples from the literature, we do not find evidence for systematic oxidation due to crystal fractionation or crustal contamination. Less evolved samples, ranging from 55 to 61 wt% SiO_2, record a range of >3 orders of magnitude in fO_2, spanning the fO_2 range recorded by all samples in our suite. Among these less evolved magmas, we find that those erupted from volcanic centers located closer to the trench, closer to the Benioff Zone, and with more geochemical evidence of subducted components in the mantle source (elevated La/Nb) result in magmas that record systematically higher fO_2. We conclude that the slab/mantle source can exert greater control on magmatic fO_2 than processes occurring in even the thickest continental crust. Thus, the fO_2 of arc magmas, and hence their calc-alkaline nature, may be inherited from the mantle.

1. Introduction

The chemistry of arc magmas is intimately linked to the generation of continents (Gill, 1981). Oxygen fugacity (fO_2) contributes to the creation of the calc-alkaline magmatic trends that typify arcs (e.g., Brounce et al., 2014; Kennedy, 1955; Osborn, 1959). Despite the observation that calc-alkaline magmas are generally more oxidized than tholeiites, no consensus exists on the oxidation mechanism. Degassing, fractional crystallization, and crustal contamination – all mechanisms of differentiation – have been suggested as possible vehicles for oxidation (e.g., Lee et al., 2005). Several studies have looked for magmatic oxidation due to degassing of C, H and S species in natural systems, but either have not observed it (Brounce et al., 2014; Cottrell and Kelley, 2011; Crabtree and Lange, 2012; de Moor et al., 2013; Kelley and Cottrell, 2012) or have discovered degassing-induced magmatic reduction (Anderson and Wright, 1972; Kelley and Cottrell, 2012; Moussallam et al., 2014; Shorttle et al., 2015). Low pressure fractional crystallization can result in moderate oxidation of less than

* Corresponding author at: Smithsonian Institution; Mineral Sciences, NHB 119; 10TH & Constitution Ave, NW, Washington, DC 20560, USA. Tel.: +1 440 725 4144; fax: +1 202 357 2476.
E-mail address: GrockeS@si.edu (S.B. Grocke).

http://dx.doi.org/10.1016/j.epsl.2016.01.026
0012-821X/

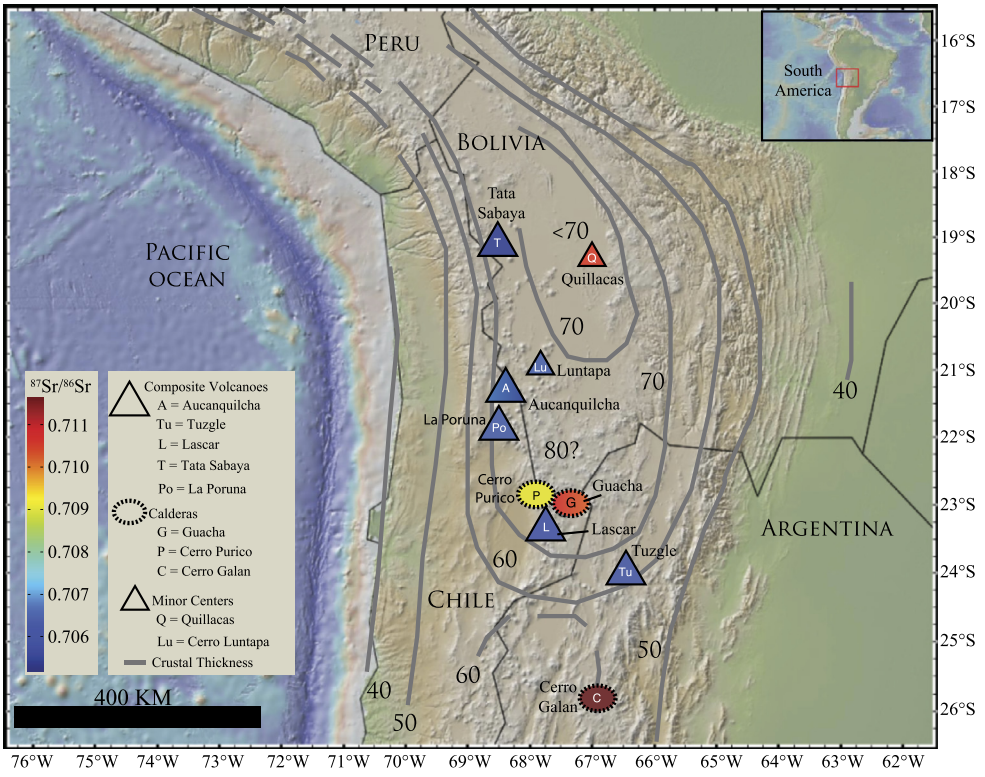

Fig. 1. The Central Volcanic Zone (CVZ) in the Andes of South America. Centers sampled span the entire CVZ and represent the complete range of $^{87}Sr/^{86}Sr$ ratios as shown in the legend. Numbers refer to crustal thickness and are from Allmendinger et al. (1997). Base map from www.geomapapp.org, Ryan et al. (2009).

half a log unit (Cottrell and Kelley, 2011) but cannot explain the disparity between the oxidation states of oceanic arc and mid-ocean ridge rocks (Brounce et al., 2014; Crabtree and Lange, 2012; Kelley and Cottrell, 2012). Crustal contamination (assimilation or partial melting of the host rock) can serve to reduce magmas (e.g., Hine et al., 1978), oxidize magmas (e.g., Ague and Brimhall, 1988), or produce no net change in oxidation state (e.g., Chappell and White, 2001), depending on the composition of the material being assimilated. The effects of crustal contamination on magmatic fO_2 are therefore not easily generalized and remain understudied. At continental arcs these processes have not been systematically evaluated and may operate to modify magmatic fO_2.

To investigate an end-member case, we examine the hypothesis that Central Andean magmas derive their oxidized nature from differentiation within an extremely thick continental crust. We focus on volcanic samples from the Central Volcanic Zone (CVZ) of the Andes in South America, where magmas have ascended through up to 80 km of continental crust (Fig. 1). CVZ volcanic rocks under consideration here have undergone variable amounts of differentiation as measured by their silica contents (basaltic andesite to rhyolite with ~55–74 wt% SiO_2; Tables 1 and 2) and radiogenic strontium isotopes ($^{87}Sr/^{86}Sr$ = ~0.705–0.712, Table 1; Davidson et al., 1991; Davidson and de Silva, 1995; Folkes et al., 2013; Kay et al., 2011; Trumbull et al., 1999).

We use two proxies for fO_2 to evaluate the oxidation state of arc magmas from the CVZ: the $Fe^{3+}/\Sigma Fe$ ratio (where $\Sigma Fe = Fe^{3+} + Fe^{2+}$) as determined on bulk rocks by wet chemistry or as measured directly in glassy melt inclusions using Fe K-edge X-ray absorption near-edge structure (XANES) spectroscopy, and the fO_2 determined from magnetite–ilmenite pairs. We provide quantitative documentation of the effect of differentiation on the fO_2s recorded by CVZ magmas. We explore the extent to which crustal processes versus modifications to the mantle wedge may be responsible for inducing calc-alkaline magmatism.

2. Geologic background

The present N–S oriented cordillera of the Andes is the result of ~200 My of subduction of the Nazca plate (Fig. 1). The Central Volcanic Zone, or CVZ, of the Central Andes lies above exceptionally thick crust (up to 80 km; Beck et al., 1996; Yuan et al., 2002; Appendix A.1), created by horizontal shortening of a thermally softened lithosphere, which uplifted the Altiplano–Puna plateau (Allmendinger et al., 1997; Isacks, 1988). Intense and voluminous caldera-forming eruptions formed the Altiplano–Puna Volcanic Complex (APVC; de Silva, 1989a; de Silva et al., 2006). The dominantly dacitic ignimbrites throughout the Central Andean Neogene Ignimbrite Province, with basaltic andesite as a minor component, belong to a high-K, calc-alkaline suite and have chemical and isotopic characteristics that suggest subduction-related mafic magmas variably contaminated by continental crust, the most contaminated being those in the APVC (de Silva et al., 2006; Folkes et al., 2013; Kay et al., 2011; Ort et al., 1996; Appendix A.1). "Baseline" isotopic compositions of $^{87}Sr/^{86}Sr$ ratios of ~0.706 and $^{144}Nd/^{143}Nd$ ratios of ~0.5124 record minimal crustal contamination (Burns et al., 2015; Davidson et al., 1991; de Silva et al., 2006; Hildreth and Moorbath, 1988). Extension of the baseline compositions to more "crustal" values indicates the significant leverage that continental crust exerts on isotopic compositions, with some extreme CVZ magmas nearing assimilant compositions (Fig. 2; de Silva, 1989b; Hawkesworth et al., 1982; Klerkx et al., 1977).

3. Geochemistry of CVZ magmas and sample selection

We chose samples that represented the maximum possible range of crustal differentiation in the CVZ. The samples represent 10 different volcanic centers and capture a large range of eruptive styles and products, compositions, and crystal contents (Table 1; Table A.1). We selected petrographically and geochemically well-

Table 1
CVZ volcanic systems sampled with composition and petrographic information.

Source	Volcano/ Caldera	Ref Sym[b]	Deposit	Sample #	Eruptive phase	Sample material	Comp	SiO_2 (wt%)	$^{87}Sr/^{86}Sr$ (error)	Crystal (%)	Phenocryst assemblage	Comments
Calderas	Guacha Caldera	Gf	Tara Fall	09008	Plinian	Pumice	Rhy	73.91[a]	0.710281(11)[a]	10	plg > qtz >> bt > pyx > ksp > ilm > zr, ap	White
		Gig	Tara IG	LA1	Ignimbrite	Pumice	Rhy	70.69	0.710562(13)[a]	30	plg > qtz > am > bt > ksp > MI >> zr, ap	Orange
	Purico	P	Purico Fall	09006	Plinian	Pumice	Rhy	69.43[a]	0.70901(25)	10	plg > bt > am > opx >> ap, zr	White
	Cerro Galan	Cn	North Dome	CG11ND	Dome	Lava	RhyDac	68.54[a]	0.711606(10)	35	plg > qtz > bt > ksp >> MI > ap, zr	Reddish/Orange
		Ce	Eagle Rock	CG11ER	Ignimbrite	Pumice	RhyDac	69.24[a]	0.711606(10)	40	plg > qtz > bt > ksp >> MI > ap, zr	Reddish/Orange
		Cf	Fan	CG11FAN	Ignimbrite	Pumice	RhyDac	69.60[a]	0.711606(10)[a]	30	plg > qtz > bt > ksp >> MI > ap, zr	Reddish/Orange
		Cd	Dome 2	CG11D2	Dome	Lava	RhyDac	70.54[a]	0.711606(10)	40	plg > qtz > bt > ksp >> MI > ap, zr	Blk; fresh, glassy
Composite Volcanoes	La Poruna	Po	Cinder Cone	09001	Flow	Lava	And	59.01[a]	0.706385(10)[a]	25	plg > opx > cpx > ol	Black
	Lascar	Lc	1993 Tephra	LA09009_3	Flow	Pumice_core	And	60.56	0.706638(11)	20	plg > opx > cpx > bt > MI >> ap, zr	Red
		Lm	1993 Tephra	LA09009_2	Flow	Pumice_mid	And	60.56	0.706638(11)	20		Orange
		Lr	1993 Tephra	LA09009_1	Flow	Pumice_rim	And	60.56	0.706638(11)	20		White
		Lp	1993 Tephra	LA09009	Flow	Pumice	And	60.56[a]	0.706638(11)[a]	20		Red core white rim
		Ls	1993 Tephra	LA09010	Flow	Scoria	And	58.63	0.706281(13)[a]	20	plg > opx > cpx > bt > MI >> ap, zr	Blk
		Lf	Soncor	LA124	Ignimbrite	Scoria	Bas And	56.83	0.706242	20	plg > cpx > ol > MI > opx >> ap, zr	Blk
	Tuzgle	Tu	Young Flow	Tuzgle	Flow	Lava	And	59.24	0.70628(16)	12	ol > am > bt > MI	mm; xeno
	Aucanquilcha Volcanic Cluster	Ap	Polan-Central	AP0736	Flow	Lava	And	60.70	0.706780(8)	15	plg > cpx > am > opx >> bt, ol, MI, zr	Blk; mm; xeno
		Ag	Gordo-Rojo	AP0729	Flow	Lava	And	59.10	0.70626(1)	15	plg > cpx > opx > am >> ol, zr	
	Tata Sabaya	T	Stage 3	TS9025	Debris Flow	Lava	Bas And	57.60	0.70516(9)	45	plg > am > cpx > MI >> ol > ap-zr	Blk; alt oxides
Mafic Centers	Bolivian Minor Centers	Lu	Cerro Luntapa	BC9005	Flow	Lava	Bas And	54.78	0.706170(17)	5	plg > pyx > ol > mg	Blk; glassy; xeno
		Q	Quillacas	BC9024	Flow	Lava	And	61.35	0.710440(28)	5	plg > pyx > am > ol	Blk; glassy; mm

[a] Values determined in this study;
[b] First letter refers to volcanic center (Fig. 1), second letter to erupted unit. mm = magma mingling; xeno = xenocrysts; alt = altered; plg = plagioclase; qtz = quartz; bt = biotite; pyx = pyroxene; ksp = K-feldspar; zr = zircon; ap = apatite; MI = magnetite + ilmenite; mg = magnetite; ilm = ilmenite; ol = olivine.

Table 2
Whole rock major element compositions calculated anhydrous.

Volcano	Guacha Caldera/Tara Deposits			La Poruna	Purico	Cerro Galan				Aucanquilcha	
Sample	09008[a]	09008[b]	LA1[a]	09001[a]	09006[a]	CG11ND[a]	CG11ER[a]	CG11FAN[a]	CG11D2[a]	AP0736[d]	AP0729[d]
Ref Sym	Gf	Gf (MIs)	Gig	Po	P	Cn	Ce	Cf	Cd	Ap	Ag
SiO_2	73.91	77.00	70.69	59.01	69.43	68.54	69.24	69.60	70.54	60.70	59.10
TiO_2	0.30	0.09	0.50	0.79	0.47	0.66	0.56	0.56	0.56	1.05	1.05
Al_2O_3	13.64	12.97	15.20	16.61	15.99	15.38	15.66	15.20	15.21	16.50	16.60
FeO^T	2.61	0.76	2.76	6.10	2.90	3.23	2.83	2.80	2.38	5.65	6.61
MnO	0.07	0.05	0.06	0.10	0.08	0.05	0.05	0.04	0.03	0.09	0.11
MgO	0.39	0.07	0.94	5.08	0.88	1.27	1.06	1.17	0.60	3.04	3.66
CaO	1.90	0.82	2.58	6.40	3.20	2.78	2.50	2.60	2.39	5.73	5.89
Na_2O	2.42	2.94	2.84	3.85	3.47	3.45	3.25	3.20	3.41	4.15	3.75
K_2O	4.65	5.09	4.33	1.85	3.37	4.39	4.65	4.60	4.68	2.77	2.95
P_2O_5	0.11	0.01	0.11	0.20	0.19	0.25	0.21	0.18	0.20	0.36	0.32
Unnormalized Total	91.92	93.74	97.26	98.75	95.04	98.56	96.69	96.80	98.76	99.02	98.79
LOI	6.82	–	–	0.41	4.24	0.31	1.75	2.20	0.45	0.59	0.84

Volcano	Tuzgle	Lascar					Minor Centers		Tata Sabaya
Sample	Tuzgle[c]	LA09009[a]			LA09010[a]	LA124[e]	BC9005[f]	BC9024[f]	TS9025[g]
Ref Sym	Tu	Lp	Lr	Lc	Ls	Lf	Lu	Q	T
SiO_2	59.24	60.56			58.63	56.83	54.78	61.35	57.60
TiO_2	1.38	0.72			0.78	1.00	1.25	1.11	1.40
Al_2O_3	16.22	16.77			16.52	16.71	16.55	16.40	16.98
FeO^T	6.17	5.86			6.44	7.14	7.75	5.04	6.78
MnO	0.10	0.11			0.12	0.11	0.14	0.10	0.10
MgO	3.97	3.86			4.92	5.88	5.66	3.77	3.27
CaO	5.67	6.47			7.39	7.00	7.51	5.47	6.00
Na_2O	3.55	3.51			3.42	3.68	3.71	2.89	4.35
K_2O	3.22	1.94			1.59	1.41	2.25	3.52	3.00
P_2O_5	0.47	0.19			0.19	0.25	0.41	0.34	0.52
Unnormalized Total	99.32	99.76			98.89	98.88	98.69	99.10	99.15
LOI	–	09009	09009_1_rim	09009_3_core	0.03	–	0.46	0.57	0.78
		0.02	1.35	0.60					

[a] Values determined in this study.
[b] Average major element composition of melt inclusion derived from Tara fall pumice.
[c] Coira and Kay (1993).
[d] Walker et al. (2010; 2013).
[e] Matthews et al. (1999) and Gardeweg et al. (1998).
[f] Davidson and de Silva (1995).
[g] de Silva et al. (1993).

characterized samples, including lavas, pumice, and scoria (Fig. 1), and apply strict criteria to ensure that samples record magmatic $Fe^{3+}/\Sigma Fe$ ratios (section 6.2). The locations of all volcanic centers sampled, as well as their tectonic setting, age, and volume, are provided in Table A.1. In Table 1, we provide information on the specific samples analyzed, including composition, crystal content, phenocryst assemblage, and a visual description of sample color. Our decision to have all analyses (majors, traces, isotopes, $Fe^{3+}/\Sigma Fe$ ratios) derive from the same parent sample resulted in analysis of a single sample from each volcanic center. We place our samples within the broader geochemical context of the volcanic centers from which they derive (Appendices A.2 and A.3; Figs. A.3, A.4, A.5). We present a statistical analysis that explores the potential impact of our study design on our conclusions that justifies our approach to assessing whether SiO_2 varies systematically with fO_2 as it does with major and minor elements (Appendix A.4; Fig. A.6).

4. Analytical methods

4.1. Whole rock geochemistry and isotopes

We determined major element compositions of ten bulk samples by X-ray Fluorescence (XRF) at the Washington State University GeoAnalytical Lab. We combine whole rock major elements new to this study with analyses reported from the literature (Table 2). We analyzed Sr isotopes on six samples using thermal ionization mass spectrometry (TIMS) at New Mexico State University. Other values are from the literature (Table 1). We provide analytical details in Appendix A.5.

4.2. Determinations of $Fe^{3+}/\Sigma Fe$ ratios

4.2.1. Wet chemistry

We analyzed the Fe^{2+} (FeO wt%) concentration in variably crystalline samples in duplicate using microcolorimetry (Carmichael, 2014). We crushed each sample in a ceramic ball mill at the Smithsonian Institution to achieve well-mixed powders and followed the procedures of Cottrell and Kelley (2011), based on the procedure of Carmichael (2014). We combined these data with measurements of total iron (FeO*) on the same samples by XRF to obtain $Fe^{3+}/\Sigma Fe$ ratios.

4.2.2. XANES

We obtained Fe K-edge X-ray absorption near-edge structure (XANES) spectra at station X26A at the National Synchrotron Light Source (NSLS), Brookhaven National Laboratory (BNL), to determine $Fe^{3+}/\Sigma Fe$ ratios in homogeneous, glassy, naturally quenched, crystal-free quartz-hosted melt inclusions. Seven rhyolitic glasses with known $Fe^{3+}/\Sigma Fe$ ratios served as standards (Cottrell et al., 2009 and Appendix A.5).

4.3. Determinations of fO_2

4.3.1. Fe–Ti oxide geothermometry and oxygen-barometry

We determined major element compositions of coexisting titanomagnetite and ilmenite grains in thin section using the JEOL-

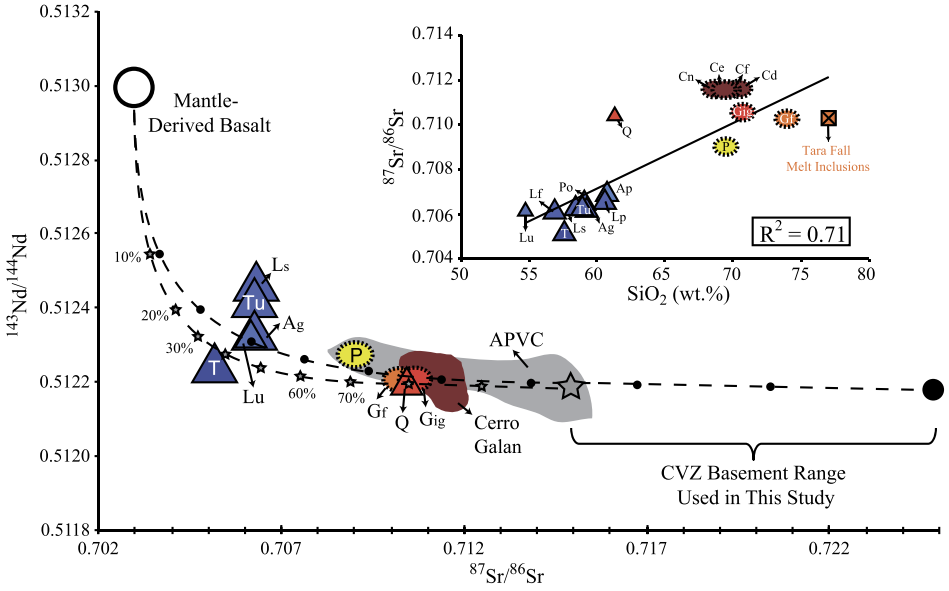

Fig. 2. Sr–Nd isotopic data for Central Volcanic Zone samples analyzed in this study. Reference symbols correspond with those listed in Fig. 1 and Table 1, based on magma source (composite volcanoes are large triangles, calderas are ovals, and minor centers are small triangles) and eruptive unit. The field of Altiplano–Puna Volcanic Complex (APVC) magmas includes the Western APVC magmas from Schmitt et al. (2001) and Lindsay et al. (2001). Field for Cerro Galan includes samples from Francis and Sparks (1989). Starting mantle-derived basalt composition from Schmitt et al. (2001). Simple mixing models are shown using assimilation-fractional crystallization modeling (DePaolo, 1981) with progressive amounts of crustal mixing (10% increments) with a basaltic magma. Two models are shown using the range in basement endmember compositions (represented by the large star and large filled circle) presented by Lucassen et al. (2001; Appendix A.1). Inset figure shows $^{87}Sr/^{86}Sr$ versus SiO_2 content for the samples selected in this study. Compiled whole rock major element compositions for each sample are listed in Table 2. All samples are color-coded based on their $^{87}Sr/^{86}Sr$ content (see scale bar in Fig. 1). (For interpretation of the references to color in this figure legend, the reader is referred to the web version of this article.)

8900 electron microprobe at the Smithsonian Institution (Table A.2; Appendix A.5). We applied the recalculation procedure of Stormer (1983) and the thermometers of Andersen and Lindsley (1988) and Ghiorso and Evans (2008) to calculate temperature and fO_2 of the CVZ magmas that crystallized Fe–Ti oxides.

4.3.2. *Kress and Carmichael (1991) calibration*

Using major oxide composition from XRF in combination with temperatures obtained from this study or the literature using mineral thermometry (e.g., Fe–Ti oxides, two-pyroxenes, plagioclase-amphibole pairs), we use the Kress and Carmichael (1991) calibration (eq. 6) to calculate fO_2 (relative to the NNO buffer of Frost, 1991) from $Fe^{3+}/\Sigma Fe$ ratios. These calculations are only strictly valid for quenched liquids because solid assemblages can have variable $Fe^{3+}/\Sigma Fe$ ratios at a given fO_2 due to the crystal chemical constraints imposed by mineral stoichiometry (e.g., McCanta et al., 2004). Despite this, the Kress and Carmichael (1991) model has been frequently applied to partially crystalline rocks (e.g., Table 2 in Carmichael, 1991; Table 3 in Crabtree and Lange, 2012) and can yield fO_2 consistent with Fe–Ti oxides (Crabtree and Lange, 2012). Crabtree and Lange (2012) showed that partial crystallization of lavas from the Tequila volcanic field occurred primarily during rapid "closed system" groundmass crystallization and that this preserves the $Fe^{3+}/\Sigma Fe$ ratio. The andesites and basaltic andesites from the CVZ are dominantly aphyric with glassy groundmass; we therefore expect the Kress and Carmichael (1991) relationship between $Fe^{3+}/\Sigma Fe$ ratio and fO_2 to hold. In the cases of the frothy ignimbrite dacite and rhyolite pumices and the crystal rich lavas, we compare our bulk rock fO_2 results with estimates from Fe–Ti oxides to ensure that the Kress and Carmichael (1991) model yields fO_2 consistent with Fe–Ti oxides.

5. Results

5.1. Whole rock geochemistry and isotopes

Whole rocks provide a range in SiO_2 concentrations (54.78–73.91 wt%, calculated anhydrous) and measured $^{87}Sr/^{86}Sr$ ratios (0.70516 to 0.71160; Table 1; Fig. 2; correction to initial values is small and can be neglected). The most differentiated samples in the suite are from the APVC and Cerro Galan caldera systems; they have the highest $^{87}Sr/^{86}Sr$ ratios (~0.709 to 0.712) and SiO_2 concentrations (~69 to 74 wt%; Table 1; Figs. 2, A.3, A.4, A.5). Basaltic andesites and andesites from CVZ composite volcanoes and Bolivian minor centers have the lowest $^{87}Sr/^{86}Sr$ ratios (~0.705 to 0.707) and SiO_2 concentrations (~55 to 61 wt%), with the exception of the Quillacas andesite that has an elevated $^{87}Sr/^{86}Sr$ ratio (0.710440, Table 1, Fig. 2). SiO_2 (wt%) correlates with $^{87}Sr/^{86}Sr$ ratios ($R^2 = 0.71$; inset in Fig. 2). The correlation between isotopic ratios and SiO_2 content makes it difficult to distinguish between the effects of crystallization and crustal contamination on the compositions of erupted magmas (Appendix A.2). For this reason, our discussion is presented in terms of the overall extent of differentiation, which includes crystal fractionation as well as crustal contamination, whether by partial melting or assimilation.

5.2. $Fe^{3+}/\Sigma Fe$ ratios

5.2.1. *Wet chemistry*

Whole rock samples from the CVZ span a range in $Fe^{3+}/\Sigma Fe$ ratios (0.19 to 0.54; Table 3). Importantly, the basaltic andesites and andesites bracket the entire range of $Fe^{3+}/\Sigma Fe$ ratios recorded by our sample suite, including the highly differentiated magmas that display a narrower range of $Fe^{3+}/\Sigma Fe$ ratios (between 0.42 and 0.48). Further, across the spectrum of differentiation, we found CVZ samples with $Fe^{3+}/\Sigma Fe$ ratios as low, or even lower, than those found in the ocean–ocean convergent margin basalts of the Marianas. We discuss separately below whole rock samples from two systems (Lascar and Cerro Galan) that show distinct signs of post-eruptive alteration (e.g., visibly zoned pumice, and crystal rich orange lavas, respectively) to quantify the effect of alteration on the fO_2 of bulk rocks. These sub-samples have $Fe^{3+}/\Sigma Fe$ ratios that reach 0.84 ± 0.05 (Table 3) and were not included in our final discussion. This exercise is useful, however, in demonstrating the potential magnitude of post-eruptive oxidation.

Table 3
Measurements of wt.% FeO, ΔNNO, and $Fe^{3+}/\Sigma Fe$ on bulk rocks, Fe–Ti oxides, and melt inclusions.

Volcano	Sample	Reference symbol	Colorimetry $Fe^{3+}/\Sigma Fe$ Avg. ± 1σ	Colorimetry ΔNNO Avg. ± 1σ	Colorimetry wt% FeO Avg. ± 1σ	Fe–Ti Oxides (pre-eruptive) wt% FeO Avg. ± 1σ	Fe–Ti Oxides (pre-eruptive) $Fe^{3+}/\Sigma Fe$ Avg. ± 1σ	Δ wt% FeO (Fe–Ti oxides – colorimetry)	FeO* (wt%)
Samples that show signs of post-eruptive alteration									
Post CG IG	CG11ND	Cn	0.84 ± 0.05	6.69 ± 0.90	0.50 ± 0.17	2.11 ± 0.20	0.35 ± 0.06	1.61	3.23
Post CG IG	CG11ER	Ce	0.78 ± 0.01	5.72 ± 0.18	0.62 ± 0.04	1.71 ± 0.08	0.40 ± 0.03	1.09	2.83
Post CG IG	CG11FAN	Cf	0.29 ± 0.09	0.86 ± 0.93	1.99 ± 0.24	1.65 ± 0.03	0.41 ± 0.01	−0.34	2.80
Lascar	09009_3_Core	Lc	0.40 ± 0.03	2.06 ± 0.26	3.54 ± 0.17	4.02 ± 0.03	0.31 ± 0.01	0.48	5.86
Lascar	09009_2_Middle	Lm	0.39 ± 0.02	2.05 ± 0.17	3.55 ± 0.11				5.86
Lascar	09009	Lp	0.38 ± 0.04	1.95 ± 0.35	3.61 ± 0.22				5.86
Samples used in interpretation									
Tara Fall	09008[a]	Gf	0.367 ± 0.003[a]	1.64 ± 0.00[a]	0.49 ± 0.00[a]				0.76[a]
Tara Ignimbrite	LA1	Gig	0.42 ± 0.02	2.32 ± 0.19	1.59 ± 0.06	1.99 ± 0.02	0.28 ± 0.01	0.40	2.76
Cerro Purico Fall	09006	P	0.48 ± 0.05	2.84 ± 0.47	1.50 ± 0.15	1.82 ± 0.02	0.37 ± 0.01	0.32	2.90
Post CG IG	CG11D2	Cd	0.42 ± 0.03	2.17 ± 0.27	1.37 ± 0.07	1.41 ± 0.03	0.41 ± 0.01	0.04	2.38
La Poruna	09001	Po	0.27 ± 0.01	0.84 ± 0.12	4.45 ± 0.07				6.10
Lascar	09009_1_Rim	Lr	0.32 ± 0.03	1.29 ± 0.32	4.01 ± 0.19	4.02 ± 0.07	0.31 ± 0.01	0.01	5.86
Lascar	09010	Ls	0.33 ± 0.03	1.37 ± 0.33	4.34 ± 0.21				6.44
Lascar	LA124	Lf	0.30 ± 0.08	1.15 ± 0.86	4.41 ± 0.13				7.06
Tuzgle	TUZGLE	Tu	0.19 ± 0.01	−0.34 ± 0.18	4.99 ± 0.08	4.52 ± 0.48	0.26 ± 0.08	−0.47	6.13
Aucanquilcha	AP0736	Ap	0.54 ± 0.01	3.15 ± 0.03	2.61 ± 0.02	4.32 ± 0.42	0.25 ± 0.07	1.71	5.65
Aucanquilcha	AP0729	Ag	0.34 ± 0.02	1.48 ± 0.19	4.35 ± 0.13				6.61
Tata Sabaya	TS9025	T	0.40 ± 0.02	1.98 ± 0.28	4.03 ± 0.21				6.72
Cerro Luntapa	BC9005	Lu	0.49 ± 0.01	2.85 ± 0.01	3.92 ± 0.01				7.65
Quillacas	BC9024	Q	0.26 ± 0.02	0.67 ± 0.26	3.68 ± 0.12				4.98

Standards	Avg Colorimetry (wt% FeO)	Certified (wt% FeO)	(Average colorimetry – certified values) (wt% FeO)
BCR-1	9.03 (0.23)	8.80	0.23
QLO-1a	3.21 (0.24)	2.97	0.24
BIR-1a	8.62 (0.18)	8.34	0.28

All analyses performed in duplicate. Duplicate standards run with each analytical session. The average standard value is reported. $\Delta NNO = \log fO_2$ (sample) – $\log fO_2$ (Ni–Ni buffer) at temperature reported in Table A.2 using Andersen and Lindsley (1988). wt% FeO from bulk rock was converted to ΔNNO using the Kress and Carmichael (1991) model (eq. (6)).

[a] All analyses of sample 09008 were conducted on a quartz-hosted melt inclusion using XANES (XRF for FeO*).

5.2.2. XANES

Despite efforts to acquire XANES data on quartz-hosted melt inclusions in high-silica rhyolites and olivine-hosted melt inclusions in basaltic andesites, only pumice from the Tara fallout deposit erupted from the Guacha II Caldera in SW Bolivia (77.0 wt% SiO_2; Figs. 1 and 2; Table 1) yielded naturally glassy inclusions ($n = 2$) that we were able to analyze via spectroscopic techniques (Fig. A.7). Many additional quartz-hosted inclusions appeared petrographically to be perfectly glassy; however, XANES spectra revealed ordering in the XAFS region indicative of nano-scale crystallization or devitrification (Fig. A.8). Multiple analyses of two naturally quenched, glassy, quartz-hosted melt inclusions, free of daughter crystals and vapor bubbles, in the Tara rhyolite fallout pumice ($^{87}Sr/^{86}Sr$ value of 0.710281; Table 1) gave an average $Fe^{3+}/\Sigma Fe$ ratio of 0.367 ± 0.003 (Table 3).

5.3. Fe–Ti oxide geo-thermometry and oxygen-barometry (fO_2)

Fe–Ti oxides from individual CVZ samples yield a narrow range in temperature and fO_2 that fall within the equilibrium test of Bacon and Hirschmann (1988; Fig. A.9; Table A.2). Using the calibration of Andersen and Lindsley (1988), magmatic temperatures range from 803 to 906 °C for all samples, with an average two-sigma standard deviation of ±13 °C (Table A.2; Fig. A.10). Pre-eruptive ΔNNO values range from +0.6 to +2.1 (Table A.2, Figs. A.10 and A.11). Use of the Ghiorso and Evans (2008) formulation does not change our conclusions and, like several other workers (e.g., Blundy et al., 2008; Folkes et al., 2011; Wright et al., 2011), we prefer the Anderson and Lindsley (1988) formulation (see Appendix A.6). We provide and discuss results using both formulations (Appendix A.6; Table A.2; Fig. A.12), but employ results from Anderson and Lindsley (1988) in the main text.

6. Discussion

6.1. Effects of syn- and post-eruptive alteration

The oxidation state of Fe (i.e., $Fe^{3+}/\Sigma Fe$ ratio) in volcanic rocks has been applied extensively as an fO_2 proxy (e.g., Bézos and Humler, 2005; Carmichael, 1991; Christie et al., 1986; Cottrell and Kelley, 2011; Crabtree and Lange, 2012), with the understanding that care must be taken to ensure that post-eruptive alteration is not a factor. For example, bulk samples such as pumice (frothy glass with a high surface area), ignimbrites (gas-particulate flows that incorporate air while hot), or rocks that contain olivine with visible iddingsite rims, must not be used to infer magmatic fO_2 (e.g., Carmichael, 1991; Crabtree and Lange, 2012); however, the effect of syn- and post-eruptive oxidation has not been quantified. CVZ samples exhibit a range in alteration textures, enabling us to quantify the effect of alteration on the fO_2 derived from whole rock analysis. We analyzed Fe–Ti oxides when we had reason to be suspicious of any bulk rock sample, due its high crystallinity, visible alteration, or frothy texture, which included pumice samples (e.g., Lascar, Purico, and Guacha) and crystal-rich and/or altered lavas (e.g., Cerro Galan and Tuzgle).

To quantify the effect of syn- or post-eruptive alteration on bulk rock fO_2, we compare $Fe^{3+}/\Sigma Fe$ ratios derived from whole rock and Fe–Ti oxides measured in two dacite post-collapse lavas (samples CG11ND, CG11D2) and two ignimbrites (samples CG11ER, CG11FAN) from Cerro Galan. These samples have similar ages, compositions, and likely erupted from the same volcanic system, but represent different styles of eruption.

The Dome 2 lava (sample CG11D2) has no visible oxidation, and has a black, glassy groundmass (Table 1). In contrast, North Dome (sample CG11ND) has a distinct reddish color visible in hand sample (Fig. A.13). $Fe^{3+}/\Sigma Fe$ ratios from whole rock analysis and

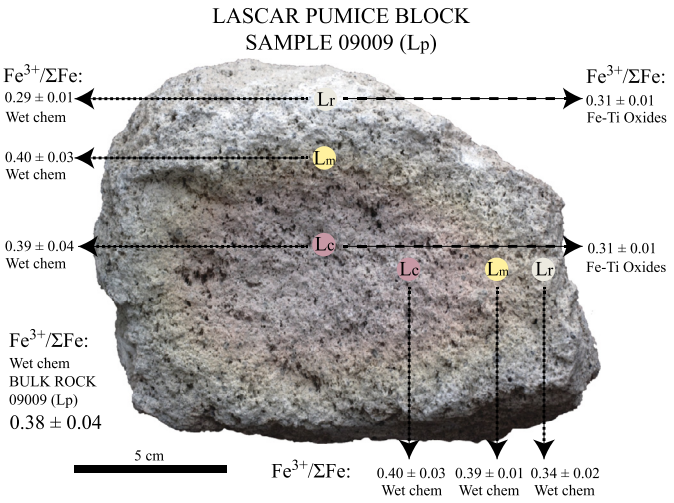

Fig. 3. Lascar pumice block (sample 09009) photograph with two transects with sample locations from rim to core labeled Lr (rim), Lm (middle), and Lc (core), respectively. We report $Fe^{3+}/\Sigma Fe$ ratios measured with whole rock wet chemistry and $Fe^{3+}/\Sigma Fe$ ratios calculated from Fe–Ti oxides for each respective zone. We calculate $Fe^{3+}/\Sigma Fe$ ratios from an average fO_2 derived from all pairings of magnetite and ilmenite using Kress and Carmichael (1991). Error for each analysis is 1σ.

derived from Fe–Ti oxides from Dome 2 are nearly identical, within error (0.42 ± 0.03 and 0.41 ± 0.01, respectively; Table 3), whereas the $Fe^{3+}/\Sigma Fe$ ratios determined on whole rocks for North Dome deviate from the Fe–Ti oxide values (0.84 ± 0.05 and 0.35 ± 0.06, respectively; Table 3), with the whole rock giving a significantly more oxidized $Fe^{3+}/\Sigma Fe$ ratio. This result confirms the findings of Crabtree and Lange (2012), who showed that bulk $Fe^{3+}/\Sigma Fe$ ratios of fresh, partially crystalline lava samples, like Dome 2, record pre-eruptive fO_2. Furthermore, it demonstrates that visibly altered bulk rock samples can give a post-eruptive $Fe^{3+}/\Sigma Fe$ ratio that is more than twice as oxidized as the pre-eruptive value derived from Fe–Ti oxides.

The ignimbrite samples from Cerro Galan (samples CG11ER and CG11FAN) each have a strong reddish/orange color in hand sample and elevated LOI values (1.75 and 2.20 wt%, respectively; Tables 1 and 2). The bulk rock $Fe^{3+}/\Sigma Fe$ ratios for the two ignimbrites deviate from the Fe–Ti oxide ratios consistent with an eruptive/emplacement style in which air entrained by hot particulate gas flows may cause oxidation. Interestingly, magnetite–ilmenite pairs from all Cerro Galan lavas and ignimbrites exhibit a very narrow range in temperature and fO_2 ($T = 803$ to $823\,^{\circ}C$, $\Delta NNO = +1.5$ to $+2.1$; Figs. A.10, A.11, Table A.2), predicting constrained $Fe^{3+}/\Sigma Fe$ ratios (0.35 to 0.41; Fig. A.13; Table 3). The redox homogeneity captured by Fe–Ti oxides exists despite very different emplacement and cooling histories experienced by the domes and ignimbrites and variable textures of the oxides (Fig. A.13). Those samples that show visible signs of alteration also have post-eruptive whole rock wt% FeO values that deviate from those derived from Fe–Ti oxides by as much as 1.61%, likely due to syn- or post-eruptive alteration. This initial case study shows that by comparing $Fe^{3+}/\Sigma Fe$ ratios from bulk rock and Fe–Ti oxides, we can ensure that the bulk rock fO_2 values used in interpretation are indeed magmatic and not representative of syn- or post-eruptive alteration.

We conducted a second case study to quantify the amount of bulk rock oxidation due to syn- and post-eruptive alteration, which involved the analysis of a single pumice block erupted from Lascar volcano in 1993. Pumice from the andesitic flow exhibit visible zonation with quenched white rims and reddish cores (Fig. 3). To deduce whether the apparent oxidation visually detected in the cores would be present in analysis, we performed three sets of measurements. To sample individual zones we cut core-to-rim transects and prepared thin sections from each zone (core, middle, and rim). We analyzed the compositions of touching oxide pairs within each zone and calculated $Fe^{3+}/\Sigma Fe$ ratios from oxygen fugacity using the Kress and Carmichael (1991) calibration. Bulk rock analysis of the individual zones of two transects yielded disparate $Fe^{3+}/\Sigma Fe$ ratios for the three zones (averages and 1σ error for the rim $= 0.32 \pm 0.03$, middle $= 0.39 \pm 0.02$, and core $= 0.40 \pm 0.03$; Table 3); the red core is notably more oxidized than the rapidly quenched white rim (Fig. 3). Wet chemical analysis of the entire pumice yielded a $Fe^{3+}/\Sigma Fe$ ratio of 0.38 ± 0.04, consistent with the average of wet chemical data collected on individual zones (Fig. 3; Table 3). All three zones of the pumice block have the same crystal content (~20 vol.%; Table 1), which implies that crystal content cannot explain the variations in bulk rock $Fe^{3+}/\Sigma Fe$ ratios. In contrast, Fe–Ti oxides from the rim yield a $Fe^{3+}/\Sigma Fe$ ratio that is identical to that recorded by the core ($Fe^{3+}/\Sigma Fe = 0.31 \pm 0.01$ Fig. 3; Table 3). The Fe–Ti oxide values are significantly more reduced than fO_2 estimates from the bulk rock. We conclude that syn-eruptive oxidation of pumice interiors can result in ~1 order of magnitude increase in apparent fO_2 while rapidly quenched pumice rims can record magmatic fO_2. For this reason, we only interpret bulk rock fO_2 data from the rim of the Lascar pumice that is in excellent agreement (0.01% deviation in FeO%; Table 3) with Fe–Ti oxides.

6.2. Criteria for determining values of magmatic fO_2 from each volcano

Our complete sample suite (total of 19 samples; Table 1) includes aphyric andesites and basaltic andesites, frothy ignimbrite dacite and rhyolite pumices, and crystal rich lavas, but we have shown that only a subset of these are useful for quantifying magmatic fO_2. Basaltic andesites and andesites that are included in our discussion have met all of the following criteria: 1) black in hand sample, 2) LOI values <0.9 wt% (Table 2), and 3) no mineralogical evidence of alteration. All ignimbrite pumices included in our discussion show excellent agreement between Fe–Ti oxides and bulk rock analysis (Table 3; Δ wt% FeO <0.40), though we note that Fe–Ti oxides from Tuzgle and Aucanquilcha show large variations in ΔNNO and temperature (Appendix A.7). Application of these criteria yielded 13 samples that provide robust constraints on the magmatic, pre-eruptive fO_2 using wet chemistry (Table 3). We also include results from melt inclusions derived from a single sample (09008) using spectroscopic techniques and application of the Kress and Carmichael (1991) formulation, which yield an fO_2 value of $\Delta NNO + 1.6$. Only these 14 analyses are considered in the discussion that follows.

6.3. Controls on the fO_2s of CVZ magmas

After removing the effects of alteration, two key results stand out that need to be addressed. First, the least differentiated magmas, basaltic andesites and andesites span the full range of fO_2 determined for the entire sample suite. Second, the observed range of fO_2 extends over three orders of magnitude, from values that encompass basalts from the Marianas that have experienced no crustal contamination ($\sim \Delta NNO + 0.8$) to some of the highest values yet reported for calc-alkaline volcanics ($\Delta NNO + 3.2$). To explain these observations, we explore four hypotheses that involve variations in: 1) magmatic differentiation (assimilation and fractional crystallization), 2) degassing, 3) interaction with meteoric water, or 4) mantle source conditions.

6.3.1. Differentiation

The samples in this study were selected because they range from basaltic andesite to rhyolite (54.8–73.9 wt% SiO_2; Table 1; Fig. 2) and show a range in radiogenic strontium isotopes

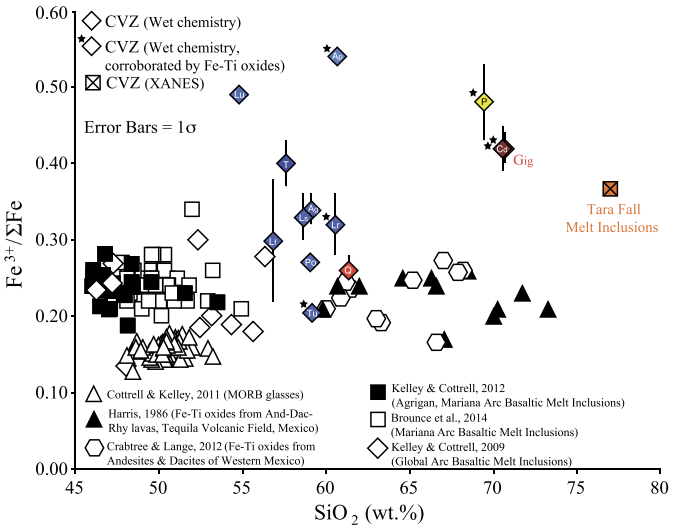

Fig. 4. Compiled $Fe^{3+}/\Sigma Fe$ ratios plotted as function of wt.% SiO_2 (after Crabtree and Lange, 2012). The *colored square* is from XANES measurements done on a single melt inclusion hosted in a quartz phenocryst from the CVZ (this study). The *colored diamonds* are wet chemistry measurements made on bulk rocks from the CVZ. Those colored diamonds with a star in the upper left, signify the samples that show agreement between Fe–Ti oxide and wet chemistry measurements (see Table 3). The melt inclusion and bulk rocks are color-coded according to their $^{87}Sr/^{86}Sr$ content (see scale bar in Fig. 1). Error bars on CVZ samples are 1σ. Open *diamonds and closed squares* are PEC-corrected melt inclusions in olivine phenocrysts from Agrigan Volcano and a global suite of arc basalts, respectively (Kelley and Cottrell, 2012, 2009). *Open hexagons* are data from Crabtree and Lange (2012) on Fe–Ti oxides from lavas from Western Mexico. *Open squares* are from Brounce et al. (2014) from Mariana arc melt inclusions in olivine phenocrysts. *Open triangles* are data from Cottrell and Kelley (2011) from a global suite of MORB glasses. *Closed triangles* are data from Harris (1986) on Fe–Ti oxides from andesite–dacite–rhyolite lavas from the Tequila Volcanic Field in Mexico. (For interpretation of the references to color in this figure legend, the reader is referred to the web version of this article.)

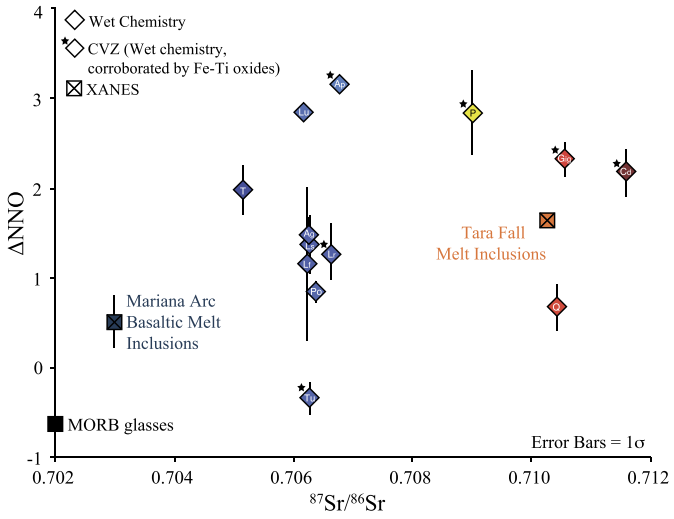

Fig. 5. Plot of ΔNNO obtained from bulk rocks and melt inclusions versus $^{87}Sr/^{86}Sr$ for samples from the CVZ. The symbols for CVZ samples are the same as in Fig. 4. All XANES and wet chemistry data referenced to ΔNNO (Frost, 1991) using Kress and Carmichael (1991). Mariana arc XANES data on olivine-hosted melt inclusions taken from Brounce et al. (2014). XANES data on MORB glasses taken from Cottrell and Kelley (2011). Samples color-coded based on their $^{87}Sr/^{86}Sr$ content (see scale bar in Fig. 1). Error bars are 1σ. (For interpretation of the references to color in this figure legend, the reader is referred to the web version of this article.)

($^{87}Sr/^{86}Sr = 0.705$–0.712; Table 1; Fig. 2). These samples therefore provide an opportunity to evaluate the effect of differentiation on $Fe^{3+}/\Sigma Fe$ ratio. We define crustal contamination either as blocks of crust falling into a molten magma body and melting into it (e.g., Fig. 1 in DePaolo, 1981) or the admixing of partial melts of pre-existing crust or wall rock induced by injected basalt sills/dikes.

Previous work on the effect of differentiation on iron oxidation state in MORB reveals either no resolvable effect (Bézos and Humler, 2005; Christie et al., 1986) or a small increase in $Fe^{3+}/\Sigma Fe$ ratios during extensive fractionation (a decrease in MgO from 10 to 6 wt% is accompanied by a 0.025 increase in $Fe^{3+}/\Sigma Fe$ ratio; Cottrell and Kelley, 2011). The low-pressure crystal fractionation trend in MORB is well modeled by fractionation of olivine or olivine ± plagioclase ± clinopyroxene in an unbuffered magma. At the Mariana Arc, Brounce et al. (2014) demonstrate that $Fe^{3+}/\Sigma Fe$ ratios from single eruptions remain constant even after extensive fractionation of olivine, clinopyroxene, plagioclase, and magnetite down to 2 wt% MgO. Similarly, Crabtree and Lange (2012) combined samples from 11 different monogenetic vents in the western Mexican volcanic arc with a larger melt inclusion dataset from Kelley and Cottrell (2009), and also concluded that crystal fractionation at arcs does not seem to systematically oxidize magmas. Finally, sample suites from Tequila (Mexico) and Pinatubo (Philippines) that range from basalt to rhyolite show no evolution in fO_2 as differentiation proceeds within a single volcanic system (Crabtree and Lange, 2012; de Hoog et al., 2004; Harris, 1986; Fig. 4).

Although the CVZ samples have undergone large extents of fractional crystallization, and show a range of $Fe^{3+}/\Sigma Fe$ ratios, many CVZ samples lie within the range of $Fe^{3+}/\Sigma Fe$ ratios defined by Mariana arc basalts and Mexican andesites and dacites (Fig. 4; Brounce et al., 2014; Cottrell and Kelley, 2011; Crabtree and Lange, 2012; Harris, 1986; Kelley and Cottrell, 2012, 2009). Moreover, we observe no trend between $Fe^{3+}/\Sigma Fe$ ratios and SiO_2. If primary SiO_2 contents are similar among the various CVZ volcanic centers, SiO_2 serves as a comparative index of differentiation (Appendix A.2). We observe an offset in fO_2 between primitive MORB and the intra-oceanic Mariana arc basalts that many attribute to the influence of subduction on the mantle wedge (e.g., Carmichael, 1991; Kelley and Cottrell, 2009; Luhr and Aranda-Gómez, 1997; Wood et al., 1990; Brounce et al., 2014). Importantly, we observe that further increases in SiO_2 beyond the Mariana arc basalts do not uniformly result in higher fO_2 as would be expected if differentiation within continental crust caused a systematic increase in fO_2. Moreover, in the CVZ, we observe no relationship between mineral assemblage (Table 1) and $Fe^{3+}/\Sigma Fe$ ratios (or fO_2). We looked in detail to see if variations in $Fe^{3+}/\Sigma Fe$ ratios observed within a set of basaltic andesites and andesites could be ascribed to phase assemblage, including major and trace phases, and found no relationship. For example, samples from both Cerro Luntapa and Quillacas, at opposite ends of the fO_2 spectrum ($\Delta NNO = +2.85$ and $+0.67$, respectively), have very similar phase assemblages (plagioclase, pyroxene, and olivine). We conclude that fractional crystallization of arc magmas does not seem to cause a systematic increase or decrease in $Fe^{3+}/\Sigma Fe$ ratios (or fO_2). Rhyolites and dacites are no more likely to be oxidized than basaltic andesites possibly due to the fact that Fe^{3+} does not act incompatibly during low-pressure crystal fractionation in these systems because Fe^{3+}-bearing spinel is on the liquidus.

We evaluate the relationship between $^{87}Sr/^{86}Sr$ ratios and ΔNNO to further quantify the effect of differentiation on fO_2 (Fig. 5). MORB and Mariana arc basalts show no continental crustal contamination and define our mantle ($^{87}Sr/^{86}Sr$ ratios ~0.702) and intra-oceanic arc ($^{87}Sr/^{86}Sr$ ratios ~0.703) baselines, respectively, whereas CVZ samples range in $^{87}Sr/^{86}Sr$ ratios from 0.705 to 0.712 (Fig. 5; Table 1). MORB samples record $fO_2 \sim \Delta NNO - 0.4$ while Mariana arc basalts are offset from MORB to higher fO_2 (average $\Delta NNO = +0.8$; Fig. 5). Again, that subduction-influenced samples (Marianas) are uniformly oxidized relative to ridge samples (MORB) (Figs. 4 and 5) is widely attributed to their origin

in the oxidized mantle wedge (e.g., Carmichael, 1991; Kelley and Cottrell, 2009; Luhr and Aranda-Gómez, 1997; Wood et al., 1990; Brounce et al., 2014). CVZ samples extend from ΔNNO $= -0.34$ ($\sim$MORB) to $+3.15$ (Fig. 5), encompassing samples that have not experienced any continental crustal contamination (e.g., MORB and Marianas). Moreover, the CVZ basaltic andesites and andesites span the entire range in fO_2 (>3 orders of magnitude) and encompass the entire range of our sample suite, including dacites and rhyolites more heavily influenced by crustal contamination. CVZ magmas nearing assimilant compositions (>70% assimilation) are no more oxidized than magmas that have experienced 30% crustal contamination. Lastly, we observe no trend between $^{87}Sr/^{86}Sr$ ratios and ΔNNO. We conclude that assimilation/melting of a single end-member basement lithology cannot account for the range of fO_2s of CVZ magmas.

We consider the ad hoc possibility that CVZ magmas leave the mantle with a given fO_2, and then assimilation/melting of multiple lithologies acts to randomly oxidize and reduce the magmas, creating the scatter in Fig. 5. The fO_2 of the basement lithologies is unknown but is likely to vary across the CVZ. On a regional scale, granites within the CVZ are predominantly I-type magmas (e.g., Suárez et al., 1990), which are more oxidized on average than S-type magmas (e.g., average $Fe^{3+}/\Sigma Fe$ ratios of I- and S-type granites from the Lachlan Fold Belt are 0.29 versus 0.15, respectively; Chappell and White, 1992). However, several studies reveal the potential of I-type magmas to assimilate/melt reduced sedimentary or metasedimentary source rocks (Ague and Brimhall, 1988; Pedersen, 1981; Rowins, 2000). Even if basement lithologies vary considerably in fO_2, the great limitation of this explanation is that the basaltic andesites and andesites that have experienced far less crustal contamination, based on Sr isotopes, would need to preferentially assimilate/melt much more oxidized lithologies than the rhyolites and dacites to produce the greater range in fO_2 that they display.

Binary mixing calculations between basalts with fO_2s similar to those found in the Mariana arc and variable assimilant compositions confirm our conclusion. To explain the more oxidized magmas, basalts would have had to have mixed with up to 30% of an assimilant at NNO +9 to produce the most oxidized basaltic andesites and andesites in our suite (Fig. A.14). The most oxidized igneous rocks described in the literature that we are aware of, minettes from Mexico, venture up to NNO +5 (Carmichael, 1991). This scenario therefore seems highly unlikely. Just as implausibly, the samples in our suite that near assimilant compositions would have had to fortuitously avoid the extremely oxidized lithologies, and only sample crust at $\sim$NNO + 2. Crustal contamination therefore appears both an unlikely and highly ad hoc explanation for the range of fO_2 in the CVZ magmas.

The idea that the surrounding country rock may impart its own fO_2 onto the CVZ magmas, independent of assimilation but rather due to diffusion of H_2 alone, has been addressed via experimental studies of disequilibrium hydration kinetics at controlled fH_2 (Gaillard et al., 2003). Gaillard et al. (2003) conclude that the communication between the redox potentials of two natural magmas (in this case the CVZ magmas and the surrounding country rock) will only affect the outermost centimeters of magma bodies such that the fO_2 of the bulk volume will not change during interactions with the surrounding environment.

6.3.2. Variable degassing

Several experimental and modeling studies conclude that water loss during equilibrium degassing will not affect magmatic $Fe^{3+}/\Sigma Fe$ ratios (e.g., Carmichael, 1991; Crabtree and Lange, 2012; Frost and Ballhaus, 1998; Gaillard et al., 2002). In contrast to these studies, Humphreys et al. (2015) suggest that H_2O degassing may oxidize magmas; however, we do not agree with this conclusion. In their unbuffered disequilibrium experiments, Humphreys et al. (2015) are measuring the effects of H_2 degassing, not H_2O degassing. They impose a fO_2 gradient, which forces H_2 to diffuse out of the capsule, oxidizing the sample. This is because H_2 alone, not H_2O, can diffuse through a platinum capsule. The Humphreys et al. (2015) results are therefore not applicable to natural systems because H_2 cannot migrate preferentially into bubbles during equilibrium degassing as it can across a platinum interface. Additional evidence that water degassing cannot drive oxidation can be found by looking at natural systems. Investigators have looked for, but not observed, an oxidative effect of degassing (of any species) on magmatic $Fe^{3+}/\Sigma Fe$ in natural systems (e.g., Brounce et al., 2014; Cottrell and Kelley, 2011; Crabtree and Lange, 2012; de Moor et al., 2013; Kelley and Cottrell, 2012; Moussallam et al., 2014; Shorttle et al., 2015). We therefore find no data to support the idea that degassing water could lead magmas to oxidize. Humphreys et al. (2015) also suggest that melt hydration may cause increases in magmatic $Fe^{3+}/\Sigma Fe$ ratios; however, equilibrium hydration of a magma, whether by addition of water or by activity changes during ascent, cannot cause an increase in $Fe^{3+}/\Sigma Fe$ ratios (Botcharnikov et al., 2005; Gaillard et al., 2001; Moore et al., 1995; see discussion in Appendix A.8).

Because the natural magmatic systems under consideration here (MORB and arc) are too oxidized to stabilize magmatic graphite, CO_2 degassing is fO_2-neutral and is not considered further (e.g., Cottrell and Kelley, 2011).

Degassing of sulfur species has the potential to oxidize or reduce magmas, but SO_2/H_2S ratios >>1 dominate subaerial degassing (e.g., Gaillard et al., 2011) and all existing data on natural systems suggests that S degassing leads to reduction (e.g., Anderson and Wright, 1972; Kelley and Cottrell, 2012; Moussallam et al., 2014; Shorttle et al., 2015). See Appendix A.8 for a detailed discussion on the effects of S degassing and gas buffering on crustal magmas.

To test the effects of degassing using data from the CVZ, we applied the model of Burgisser et al. (2015) using pre-eruptive information (see Appendix A.9) on the Tara rhyolitic magmas. The model results, from open or closed system H_2O–CO_2–S degassing, indicate that degassing will reduce the magma by $\sim$1 log unit. This result also holds for the less evolved compositions in our suite. Thus, after consideration of theoretical, numerical, and empirical arguments, we conclude that degassing is an unlikely cause of the elevated fO_2 of the CVZ samples.

6.3.3. Meteoric water

Interaction with meteoric water could potentially account for the variable fO_2 recorded by CVZ magmas. If meteoric H_2O influenced fO_2, we would expect low-$\delta^{18}O$ that records the influence of meteoric-hydrothermal events and the assimilation of hydrothermally altered crustal material. Magmatic quartz, plagioclase, and zircon crystals in CVZ ignimbrite magmas that have undergone extensive assimilation of upper continental crust (up to 50 vol.%) generally have a heavy-$\delta^{18}O$ magmatic signature that has been interpreted to reflect the limited availability and infiltration of surface meteoric water and hydrothermal alteration of the shallow crust (Folkes et al., 2013). Infiltration of meteoritic water does not therefore seem responsible for the variable fO_2 recorded by CVZ magmas. In support of this interpretation, Carmichael (1991) showed that despite extensive exchange of the ^{18}O of the silicic ash flows and lavas of Yellowstone with meteoric water following caldera collapse, there was no displacement of the redox equilibria.

6.3.4. Mantle source conditions

A striking observation is that basaltic andesites and andesites display the full range of observed fO_2 (ΔNNO $= -0.34$ to $+3.15$), yet have experienced only moderate amounts of differentiation

($^{87}Sr/^{86}Sr$ ratios <0.707, except for Quillacas that has a $^{87}Sr/^{86}Sr$ ratio of ~0.710, and yet is our second-most reduced sample). Here we address the extent to which variations in mantle source fO_2 could create the variation observed in the magmas.

Some studies have made use of ratios of fluid-mobile to fluid-immobile trace elements (e.g., Ba/La) to suggest that aqueous slab fluids are responsible for oxidizing the mantle wedge and resultant arc magmas (Kelley and Cottrell, 2009, 2012; Brounce et al., 2014). In the CVZ, however, it is difficult to evaluate the role of aqueous fluids on the fO_2 of arc magmas because fluid mobile elements such as Rb, Ba, and Pb are enriched in the continental crust (e.g., Davidson and de Silva, 1995; Kay et al., 2010; Plank, 2005; Appendix A.10). Therefore, variable degrees of crustal contamination could result in variable enrichments of each of these elements within the CVZ magmas, and potentially overwhelm fluid additions of these elements to the mantle source of the primary magmas. In contrast, prior work has shown that La/Nb (a Light Rare Earth Element/High Field Strength Element (LREE/HFSE) ratio) is a resilient mantle tracer in the Central Andes despite potential complications from the underlying overthickened continental crust (e.g., Kay et al., 2010). Similarly, we find that the La/Nb ratio of the CVZ samples remains constant despite significant variations in SiO_2 within individual volcanic centers, and therefore, like other studies in the region, we relate elevated LREE/HFSE ratios to slab influence (e.g., Kay et al., 2010; Appendix A.10; Fig. A.5).

We find that La/Nb ratios for CVZ basaltic andesites and andesites show a strong correlation with ΔNNO ($R^2 = 0.82$; p-value = .0003; Fig. 6a; Table A.3), and those magmas that have experienced more slab influence (high La/Nb) are also more oxidized. We observe supportive relationships with geophysical parameters as well. ΔNNO shows weak correlations with depth to the Benioff zone and distance to the trench ($R^2 = 0.39$, p-value = .055; $R^2 = 0.38$, p-value = .056; Figs. 6b, 6c, respectively; Table A.3), with a mild tendency of volcanic centers closer to the trench to be more oxidized. Tuzgle, for example, has the lowest ΔNNO value (−0.34) and the lowest La/Nb ratio (1.34) of the entire sample suite and sits farthest from the trench (Figs. 1 and 6). Tuzgle exhibits less of an "arc-like" affinity when compared to volcanic centers that lie along the active arc front (Coira and Kay, 1993); however the correlation between ΔNNO and La/Nb still holds when we remove Tuzgle from the suite ($R^2 = 0.71$; p-value = .003), suggesting that the relationship is not entirely due to an arc versus back arc contrast in mantle source.

There is no evidence that low-pressure crystal fractionation is controlling the La/Nb ratios of these rocks, and this is one reason that this ratio has often been employed to interrogate the sources of arc magmas in the Andes (e.g., Kay et al., 2010; Folkes et al., 2011). Few phases can fractionate La from Nb. In our sample suite, amphibole is capable of fractionating La from Nb (Parker and Fleischer, 1968); however, one sample that has a high La/Nb ratio (AP0736) and one sample that has a low La/Nb ratio (Tuzgle) both contain amphibole. There is no data to suggest that the low-pressure phase assemblage drives the relationship between La/Nb and ΔNNO.

A potential source of the variation in La/Nb ratios, and therefore fO_2 values, within the CVZ may be the volume and provenance of subducted sediments. High La/Nb, a measure of the Nb anomaly, may derive from prior mantle depletion of Nb or from the sediments via bulk addition or partial melting of subducted REE enriched sediment (Johnson and Plank, 1999; Plank, 2005). The mantle wedge beneath the Andes should not have suffered significant prior depletion because there is no back arc spreading center, and La and Nb should not fractionate during mantle melting when the melt fraction exceeds 10%, as it likely does during flux melting (Kelley et al., 2010). Volcanic centers within the CVZ may

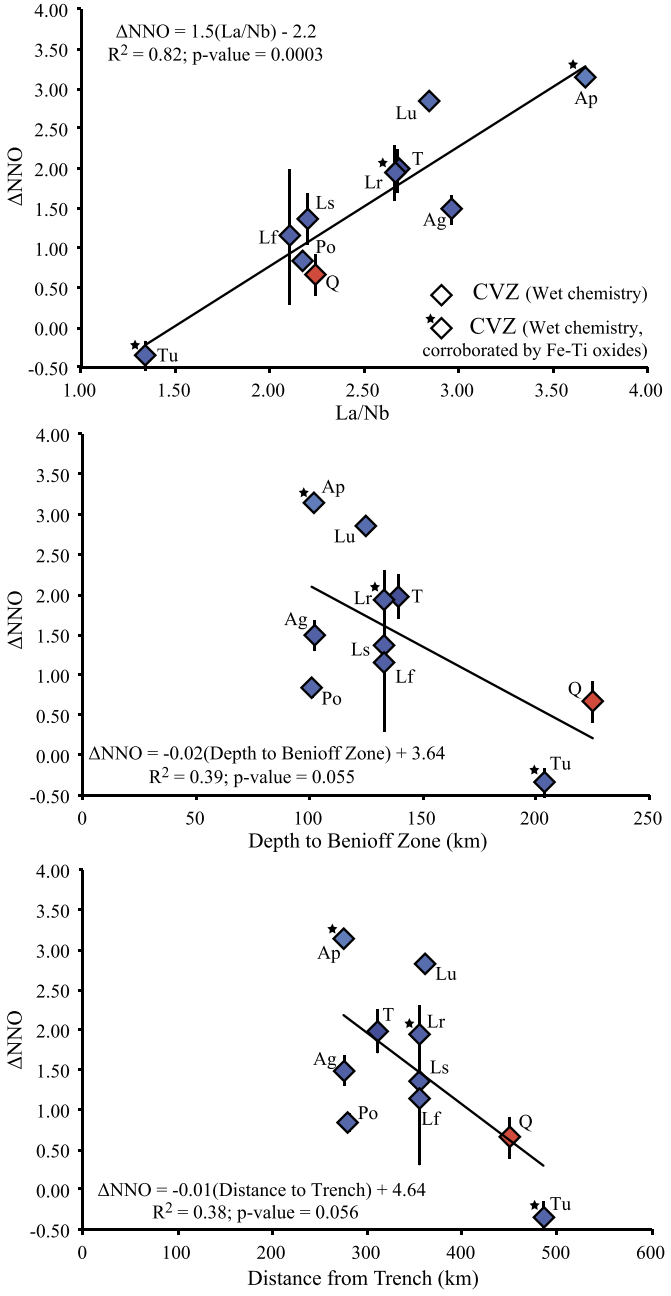

Fig. 6. CVZ andesite and basaltic andesite whole rock La/Nb ratios versus ΔNNO. The symbols for CVZ samples are the same as in Fig. 4. We report ΔNNO values calculated from bulk rock $Fe^{3+}/\Sigma Fe$ ratios. Samples color-coded based on their $^{87}Sr/^{86}Sr$ content (see scale bar in Fig. 1). Distance from trench (km) and depth to Benioff Zone (km) from Syracuse and Abers (2006). Linear regression R-squared values and p-values calculated using all data points. (For interpretation of the references to color in this figure legend, the reader is referred to the web version of this article.)

thus reflect variable additions of subducted sediment, or sediment melt. Although it is challenging to confidently apply this general reasoning in the absence of a well-characterized sedimentary sequence for this region of the arc, subducting sedimentary columns for the Chilean margin south of the CVZ show enrichment of LREE that are consistent with this interpretation (Plank, 2013) and the Andean margin has large contributions of terrigenous sediment derived predominantly by erosion from Mesozoic and Cenozoic rocks in the Andes (e.g., Hildreth and Moorbath, 1988; Stern, 1991; Plank, 2013). Because terrigenous sediments may have >80% of their iron speciated as Fe^{3+} (e.g., Lécuyer and Ricard, 1999), it is plausible that increased sediment influence at this margin would

increase both magmatic fO_2 and La/Nb ratios of CVZ magmas. In summary, the correlation between fO_2 and indicators of slab influence in the CVZ's least evolved samples suggests that magmas that have experienced more slab influence are also more oxidized.

7. Conclusions

Arc magma chemistry records myriad processes, originating in the mantle and continuing through crustal modification, eruption, emplacement, and alteration. Syn-eruptive and post-depositional processes can affect $Fe^{3+}/\Sigma Fe$ ratios. Either glassy, aphyric, black lavas must be used to constrain magmatic fO_2, or $Fe^{3+}/\Sigma Fe$ ratios from frothy pumices and crystal rich lavas must be justified and supported by data from Fe–Ti oxides or other resilient oxybarometers. There is no systematic change in the $Fe^{3+}/\Sigma Fe$ ratios of the CVZ magmas with SiO_2 concentration, consistent with previous work, and that crystal fractionation cannot account for the elevated fO_2s observed in CVZ magmas. Crustal contamination in the CVZ cannot account for the elevated fO_2s observed in CVZ magmas because it would require the least differentiated magmas to preferentially assimilate lithologies more oxidized than any yet described in the literature. Experiments, theory, and prior observations of natural systems, combined with modeling work on compositions from the CVZ, suggest that degassing leads to no change or possibly a reduction in fO_2. Therefore, degassing cannot explain our observations. Surprisingly, we observe that basaltic andesites and andesites with minimal crustal contamination display over three orders of magnitude variation in fO_2, and that this variation correlates with La/Nb ratios. Elevated La/Nb ratios may plausibly derive from bulk addition of sediment or partial melting of subducted REE enriched sediment. We propose that variable contributions from oxidized terrigenous sediment may be responsible for the fO_2s recorded by CVZ magmas. It appears that, despite extensive crustal contamination, the fO_2 recorded by CVZ magmas, and perhaps arcs globally, reflects a mantle-derived component.

Acknowledgements

We would like to thank two anonymous reviewers for providing insightful comments that significantly improved this manuscript, and Tamsin Mather for editorial handling. We appreciate assistance from T. Gooding with sample preparation, M. Brounce with wet chemistry, and T. Rose with the electron microprobe. Use of the National Synchrotron Light Source, Brookhaven National Laboratory, was supported by the U.S. Department of Energy, under contract DE-AC02-98CH10886. We acknowledge support from NSF grants EAR 0838536 and 0908324, and Smithsonian's Pre-Doctoral Fellowship and Global Volcanism Programs.

Appendix A. Supplementary material

Supplementary material related to this article can be found online at http://dx.doi.org/10.1016/j.epsl.2016.01.026.

References

Ague, J.J., Brimhall, G.H., 1988. Magmatic arc asymmetry and distribution of anomalous plutonic belts in the batholiths of California: effects of assimilation, crustal thickness, and depth of crystallization. Geol. Soc. Am. Bull. 100, 912–927.

Allmendinger, R., Jordan, T., Kay, S., Isacks, B., 1997. The evolution of the Altiplano–Puna plateau of the Central Andes. Annu. Rev. Earth Planet. Sci. 25, 139–174.

Andersen, D.J., Lindsley, D.H., 1988. Internally consistent solution models for Fe–Mg–Mn–Ti oxides: Fe–Ti oxides. Am. Mineral. 73, 714–726.

Anderson, A.T., Wright, T.L., 1972. Phenocrysts and glass inclusions and their bearing on oxidation and mixing of basaltic magmas, Kilauea volcano, Hawaii. Am. Mineral. 57, 188–216.

Bacon, C.R., Hirschmann, M.M., 1988. Mg/Mn partitioning as test for equilibrium between coexisting Fe–Ti oxides (in volcanic rocks), Am. Mineral. 73, 57–61.

Beck, S.L., Zandt, G., Myers, S.C., Wallace, T.C., Silver, P.G., Drake, L., 1996. Crustal-thickness variations in the central Andes. Geology 24, 407. http://dx.doi.org/10.1130/0091-7613(1996)024<0407:CTVITC>2.3.CO;2.

Bézos, A., Humler, E., 2005. The $Fe^{3+}/\Sigma Fe$ ratios of MORB glasses and their implications for mantle melting. Geochim. Cosmochim. Acta 69, 711–725. http://dx.doi.org/10.1016/j.gca.2004.07.026.

Blundy, J., Cashman, K.V., Berlo, K., 2008. Evolving magma storage conditions Beneath mount St. Helens inferred from chemical variations in melt inclusions from the 1980–1986 and current (2004–2006) eruptions. In: Sherrod, D.R., Scott, W.E., Stauffer, P.H. (Eds.), A Volcano Rekindled the Renewed Eruption of Mount St. Helens. In: Geol. Surv. Prof. Paper, vol. 1750.

Botcharnikov, R.E., Koepke, J., Holtz, F., McCammon, C., Wilke, M., 2005. The effect of water activity on the oxidation and structural state of Fe in a ferro-basaltic melt. Geochim. Cosmochim. Acta 69 (21), 5071–5085.

Brounce, M.N., Kelley, K.A., Cottrell, E., 2014. Variations in $Fe^{3+}/\sum Fe$ of Mariana Arc Basalts and Mantle Wedge fO_2. J. Petrol. 55, 2513–2536. http://dx.doi.org/10.1093/petrology/egu065.

Burgisser, A., Alletti, M., Scaillet, B., 2015. Simulating the behavior of volatiles belonging to the C–O–H–S system in silicate melts under magmatic conditions with the software D-Compress. Comput. Geosci. 79, 1–14.

Burns, D.H., de Silva, S.L., Tepley III, F., Schmitt, A.K., Loewen, M.W., 2015. Recording the transition from flare-up to steady-state arc magmatism at the Purico-Chascon volcanic complex, northern Chile. Earth Planet. Sci. Lett. 422, 75–86.

Carmichael, I.S.E., 1991. The redox states of basic and silicic magmas: a reflection of their source regions? Contrib. Mineral. Petrol. 106, 129–141. http://dx.doi.org/10.1007/BF00306429.

Carmichael, I.S.E., 2014. Chemical analysis of silicate rocks: a manual. EarthChem Library, 1–49.

Chappell, B.W., White, A.J.R., 1992. I-and S-type granites in the Lachlan Fold Belt. Spec. Pap., Geol. Soc. Am. 272, 1–26.

Chappell, B.W., White, A.J.R., 2001. Two contrasting granite types: 25 years later. Aust. J. Earth Sci. 48, 489–499. http://dx.doi.org/10.1046/j.1440-0952.2001.00882.x.

Christie, D.M., Carmichael, I., Langmuir, C.H., 1986. Oxidation states of mid-ocean ridge basalt glasses. Earth Planet. Sci. Lett. 79, 397–411. http://dx.doi.org/10.1016/0012-821X(86)90195-0.

Coira, B., Kay, S.M., 1993. Implications of Quaternary volcanism at Cerro Tuzgle for crustal and mantle evolution of the Puna Plateau, Central Andes, Argentina. Contrib. Mineral. Petrol. 113, 40–58. http://dx.doi.org/10.1007/bf00320830.

Cottrell, E., Kelley, K.A., 2011. The oxidation state of Fe in MORB glasses and the oxygen fugacity of the upper mantle. Earth Planet. Sci. Lett. 305, 270–282. http://dx.doi.org/10.1016/j.epsl.2011.03.014.

Cottrell, E., Kelley, K.A., Lanzirotti, A., Fischer, R.A., 2009. High-precision determination of iron oxidation state in silicate glasses using XANES. Chem. Geol. 268, 167–179. http://dx.doi.org/10.1016/j.chemgeo.2009.08.008.

Crabtree, S.M., Lange, R.A., 2012. An evaluation of the effect of degassing on the oxidation state of hydrous andesite and dacite magmas: a comparison of pre- and post-eruptive Fe^{2+} concentrations. Contrib. Mineral. Petrol. 163, 209–224. http://dx.doi.org/10.1007/s00410-011-0667-7.

Davidson, J.P., de Silva, S.L., 1995. Late Cenozoic magmatism of the Bolivian Altiplano. Contrib. Mineral. Petrol. 119, 387–408. http://dx.doi.org/10.1007/BF00286937.

Davidson, J.P., Harmon, R.S., Worner, G., 1991. The source of central Andean magmas; some considerations. Spec. Pap., Geol. Soc. Am. 265, 233–243. http://dx.doi.org/10.1130/SPE265-p233.

De Hoog, J.C.M., Hattori, K.H., Hoblitt, R.P., 2004. Oxidized sulfur-rich mafic magma at Mount Pinatubo, Philippines. Contrib. Mineral. Petrol. 146, 750–761.

de Moor, J.M., Fischer, T.P., Sharp, Z.D., King, P.L., Wilke, M., Botcharnikov, R.E., Cottrell, E., Zelenski, M., Marty, B., Klimm, K., Rivard, C., Ayalew, D., Ramirez, C., Kelley, K.A., 2013. Sulfur degassing at Erta Ale (Ethiopia) and Masaya (Nicaragua) volcanoes: implications for degassing processes and oxygen fugacities of basaltic systems. Geochem. Geophys. Geosyst. 14, 4076–4108. http://dx.doi.org/10.1002/ggge.20255.

de Silva, S.L., 1989a. Altiplano–Puna volcanic complex of the central Andes. Geology 17, 1102–1106.

de Silva, S.L., 1989b. Geochronology and stratigraphy of the ignimbrites from the 21 30′ S to 23 30′ S portion of the Central Andes of northern Chile. J. Volcanol. Geotherm. Res. 37, 93–131. http://dx.doi.org/10.1016/0377-0273(89)90065-6.

de Silva, S.L., Davidson, J.P., Croudace, I.W., Escobar, A., 1993. Volcanological and petrological evolution of volcan Tata Sabaya, SW Bolivia. J. Volcanol. Geotherm. Res. 55, 305–335. http://dx.doi.org/10.1016/0377-0273(93)90043-Q.

de Silva, S.L., Zandt, G., Trumbull, R., Viramonte, J.G., Salas, G., Jiménez, N., 2006. Large ignimbrite eruptions and volcano-tectonic depressions in the Central Andes: a thermomechanical perspective. In: Troise, C., de Natale, G., Kilburn, C.R.J. (Eds.), Mechanisms of Activity and Unrest at Large Calderas. Geol. Soc. (Lond.) Spec. Publ. 269, 47–63. http://dx.doi.org/10.1144/GSL.SP.2006.269.01.04.

DePaolo, D.J., 1981. Trace element and isotopic effects of combined wallrock assimilation and fractional crystallization. Earth Planet. Sci. Lett. 53, 189–202. http://dx.doi.org/10.1016/0012-821X(81)90153-9.

Folkes, C.B., Silva, S.L., de Wright, H.M., Cas, R.A.F., 2011. Geochemical homogeneity of a long-lived, large silicic system, evidence from the Cerro Galán caldera, NW Argentina. Bull. Volcanol. 73, 1455–1486. http://dx.doi.org/10.1007/s00445-011-0511-y.

Folkes, C.B., Silva, S.L., de Bindeman, I.N., Cas, R.A.F., 2013. Tectonic and climate history influence the geochemistry of large-volume silicic magmas: new $\delta^{18}O$ data from the Central Andes with comparison to N America and Kamchatka. J. Volcanol. Geotherm. Res. 262, 1–16. http://dx.doi.org/10.1016/j.jvolgeores.2013.05.014.

Francis, P.W., Sparks, R., 1989. Petrology and geochemistry of volcanic rocks of the Cerro Galan caldera, northwest Argentina. Geol. Mag. 126 (5), 515–547. http://dx.doi.org/10.1017/S0016756800022834.

Frost, R.B., 1991. Introduction to oxygen fugacity and its petrologic importance. In: Lindsley, D.H. (Ed.), Reviews in Mineralogy: Oxide Minerals: Petrologic and Magnetic Significance, pp. 1–9.

Frost, B.R., Ballhaus, C., 1998. Comment on "Constraints on the origin of the oxidation state of mantle overlying subduction zones: an example from Simcoe, Washington, USA". In: Brandon, A.D., Draper, D.S. (Eds.), Geochim. Cosmochim. Acta 62, 329–332.

Gaillard, F., Scaillet, B., Arndt, N.T., 2011. Atmospheric oxygenation caused by a change in volcanic degassing pressure. Nature 478, 229–232.

Gaillard, F., Schmidt, B., Mackwell, S., McCammon, C., 2003. Rate of hydrogen–iron redox exchange in silicate melts and glasses. Geochim. Cosmochim. Acta 67 (13), 2427–2441.

Gaillard, F., Scaillet, B., Pichavant, M., 2002. Kinetics of iron oxidation–reduction in hydrous silicic melts. Am. Mineral. 87, 829–837.

Gaillard, F., Scaillet, B., Pichavant, M., Bény, J.M., 2001. The effect of water and fO_2 on the ferric–ferrous ratio of silicic melts. Chem. Geol. 174 (1), 255–273.

Gardeweg, M.C., Sparks, R.S.J., Matthews, N.E., 1998. Evolution of Lascar Volcano, Northern Chile. J. Geol. Soc. London 155, 89–104. http://dx.doi.org/10.1144/gsjgs.155.1.0089.

Ghiorso, M.S., Evans, B.W., 2008. Thermodynamics of rhombohedral oxide solid solutions and a revision of the Fe–Ti two-oxide geothermometer and oxygen-barometer. Am. J. Sci. 308, 957–1039. http://dx.doi.org/10.2475/09.2008.01.

Gill, J.B., 1981. Orogenic Andesites and Plate Tectonics. Springer-Verlag, Berlin.

Harris, J.M., 1986. Silicic Volcanics of Volcan Tequila, Jalisco, Mexico. University of California, Berkeley.

Hawkesworth, C.J., Hammill, M., Gledhill, A.R., van Calsteren, P., Rogers, G., 1982. Isotope and trace element evidence for late-stage intra-crustal melting in the High Andes. Earth Planet. Sci. Lett. 58, 240–254. http://dx.doi.org/10.1016/0012-821X(82)90197-2.

Hildreth, W., Moorbath, S., 1988. Crustal contributions to arc magmatism in the Andes of central Chile. Contrib. Mineral. Petrol. 98, 455–489. http://dx.doi.org/10.1007/BF00372365.

Hine, R., Williams, I.S., Chappell, B.W., 1978. Contrasts between I- and S-type granitoids of the Kosciusko Batholith. J. Geol. Soc. Aust. 25 (3–4), 219–234. http://dx.doi.org/10.1080/00167617808729029.

Humphreys, M.C.S., Brooker, R.A., Fraser, D.G., Burgisser, A., Mangan, M.T., McCammon, C., 2015. Coupled interactions between volatile activity and Fe oxidation state during Arc crustal processes. J. Petrol. 56 (4), 795–814.

Isacks, B.L., 1988. Uplift of the Central Andean Plateau and bending of the Bolivian Orocline. J. Geophys. Res. 93, 3211–3231.

Johnson, M.C., Plank, T., 1999. Dehydration and melting experiments constrain the fate of subducted sediments. Geochem. Geophys. Geosyst. 1 (12).

Kay, S.M., Coira, B.L., Caffe, P.J., Chen, C.H., 2010. Regional chemical diversity, crustal and mantle sources and evolution of central Andean Puna plateau ignimbrites. J. Volcanol. Geotherm. Res. 198 (1), 81–111.

Kay, S.M., Coira, B., Worner, G., Kay, R.W., Singer, B.S., 2011. Geochemical, isotopic and single crystal $^{40}Ar/^{39}Ar$ age constraints on the evolution of the Cerro Galán ignimbrites. Bull. Volcanol. 73, 1487–1511. http://dx.doi.org/10.1007/s00445-010-0410-7.

Kelley, K.A., Cottrell, E., 2009. Water and the oxidation state of subduction zone magmas. Science 325, 605–607. http://dx.doi.org/10.1126/science.1174156.

Kelley, K.A., Cottrell, E., 2012. The influence of magmatic differentiation on the oxidation state of Fe in a basaltic arc magma. Earth Planet. Sci. Lett. 329–330, 109–121. http://dx.doi.org/10.1016/j.epsl.2012.02.010.

Kelley, K.A., Plank, T., Newman, S., Stolper, E.M., Grove, T.L., Parman, S., Hauri, E.H., 2010. Mantle melting as a function of water content beneath the Mariana Arc. J. Petrol. 51 (8), 1711–1738.

Kennedy, G.C., 1955. Some aspects of the role of water in rock melts. Spec. Pap., Geol. Soc. Am. 62, 489–504.

Klerkx, J., Deutsch, S., Pichler, H., Zeil, W., 1977. Strontium isotopic composition and trace element data bearing on the origin of Cenozoic volcanic rocks of the central and southern Andes. J. Volcanol. Geotherm. Res. 2, 49–71. http://dx.doi.org/10.1016/0377-0273(77)90015-4.

Kress, V.C., Carmichael, I.S.E., 1991. The compressibility of silicate liquids containing Fe2O3 and the effect of composition, temperature, oxygen fugacity and pressure on their redox states. Contrib. Mineral. Petrol. 108, 82–92. http://dx.doi.org/10.1007/BF00307328.

Lécuyer, C., Ricard, Y., 1999. Long-term fluxes and budget of ferric iron: implication for the redox states of the Earth's mantle and atmosphere. Earth Planet. Sci. Lett. 165, 197–211.

Lee, C.-T.A., Leeman, W.P., Canil, D., Li Anser, Z.-X., 2005. Similar V/Sc Systematics in MORB and Arc Basalts: implications for the oxygen fugacities of their Mantle Source Regions. J. Petrol. 46, 2313–2336. http://dx.doi.org/10.1093/petrology/egi056.

Lindsay, J.M., Schmitt, A.K., Trumbull, R.B., De Silva, S.L., Siebel, W., Emmermann, R., 2001. Magmatic evolution of the La Pacana caldera system, Central Andes, Chile: compositional variation of two cogenetic, large-volume felsic ignimbrites. J. Petrol. 42 (3), 459–486.

Lucassen, F., Becchio, R., Harmon, R., Kasemann, S., Franz, G., Trumbull, R., Wilke, H.-G., Romer, R.L., Dulski, P., 2001. Composition and density model of the continental crust at an active continental margin—the Central Andes between 21 and 27 S. Tectonophysics 341, 195–223.

Luhr, J.F., Aranda-Gómez, J.J., 1997. Mexican Peridotite Xenoliths and Tectonic Terranes: correlations among vent location, texture, temperature, pressure, and oxygen fugacity. J. Petrol. 38, 1075–1112. http://dx.doi.org/10.1093/petroj/38.8.1075.

Matthews, S.J., Sparks, R.S.J., Gardeweg, M.C., 1999. The Piedras Grandes–Soncor Eruptions, Lascar Volcano, Chile; evolution of a Zoned Magma Chamber in the Central Andean Upper Crust. J. Petrol. 40, 1891–1919. http://dx.doi.org/10.1093/petroj/40.12.1891.

McCanta, M.C., Dyar, M.D., Rutherford, M.J., Delaney, J.S., 2004. Iron partitioning between basaltic melts and clinopyroxene as a function of oxygen fugacity. Am. Mineral. 89, 1685–1693.

Moore, G., Righter, K., Carmichael, I.S.E., 1995. The effect of dissolved water on the oxidation state of iron in natural silicate liquids. Contrib. Mineral. Petrol. 120 (2), 170–179.

Moussallam, Y., Oppenheimer, C., Scaillet, B., Gaillard, F., Kyle, P., Peters, N., Hartley, M., Berlo, K., Donovan, A., 2014. Tracking the changing oxidation state of Erebus magmas, from mantle to surface, driven by magma ascent and degassing. Earth Planet. Sci. Lett. 393, 200–209. http://dx.doi.org/10.1016/j.epsl.2014.02.055.

Ort, M.H., Coira, B.L., Mazzoni, M.M., 1996. Generation of a crust-mantle magma mixture: magma sources and contamination at Cerro Panizos, central Andes. Contrib. Mineral. Petrol. 123, 308–322. http://dx.doi.org/10.1007/s004100050158.

Osborn, E.F., 1959. Role of oxygen pressure in the crystallization and differentiation of basaltic magma. Am. J. Sci. 257, 609–647. http://dx.doi.org/10.2475/ajs.257.9.609.

Parker, R.L., Fleischer, M., 1968. Geochemistry of niobium and tantalum. Geol. Surv. Prof. Paper 612.

Pedersen, A.K., 1981. Armalcolite-bearing Fe–Ti oxide assemblages in graphite-equilibrated salic volcanic rocks with native iron from Disko, central West Greenland. Contrib. Mineral. Petrol. 77, 307–324. http://dx.doi.org/10.1007/BF00371560.

Plank, T., 2005. Constraints from thorium/lanthanum on sediment recycling at subduction zones and the evolution of the continents. J. Petrol. 46 (5), 921–944.

Plank, T., 2013. The chemical composition of subducting sediments. In: Rudnick, R.L. (Ed.), The Crust. In: Treatise on Geochemistry, vol. 3, second edn. Elsevier Scientific Publishing Company, Oxford. Editors-in-chief H.D. Holland and K.K. Turekian.

Rowins, S.M., 2000. Reduced porphyry copper–gold deposits: a new variation on an old theme. Geology 28, 491.

Ryan, W.B.F., Carbotte, S.M., Coplan, J.O., O'Hara, S., Melkonian, A., Arko, R., Weissel, R.A., Ferrini, V., Goodwillie, A., Nitsche, F., Bonczkowski, J., Zemsky, R., 2009. Global multi-resolution topography synthesis. Geochem. Geophys. Geosyst. 10. http://dx.doi.org/10.1029/2008GC002332.

Schmitt, A., de Silva, S.L., Trumbull, R., 2001. Magma evolution in the Purico ignimbrite complex, northern Chile: evidence for zoning of a dacitic magma by injection of rhyolitic melts following mafic recharge. Contrib. Mineral. Petrol. 140, 680–700. http://dx.doi.org/10.1093/petrology/42.3.459.

Shorttle, O., Moussallam, Y., Hartley, M.E., Maclennan, J., Edmonds, M., Murton, B.J., 2015. Fe-XANES analyses of Reykjanes Ridge basalts: implications for oceanic crust's role in the solid Earth oxygen cycle. Earth Planet. Sci. Lett. 427, 272–285.

Stern, C.R., 1991. Role of subduction erosion in the generation of Andean magmas. Geology 19 (1), 78–81.

Stormer, J.C., 1983. The effects of recalculation on estimates of temperature and oxygen fugacity from analyses of multicomponent iron titanium-oxides. Am. Mineral. 68, 586–594.

Suárez, M., Naranjo, J.A., Puig, A., 1990. Mesozoic "S-like" granites of the central and southern Andes; a review. Spec. Pap., Geol. Soc. Am. 241, 27–32. http://dx.doi.org/10.1130/SPE241-p27.

Syracuse, E.M., Abers, G.A., 2006. Global compilation of variations in slab depth beneath arc volcanoes and implications. Geochem. Geophys. Geosyst. 7 (5), 1–18. http://dx.doi.org/10.1029/2005GC001045.

Trumbull, R.B., Wittenbrink, R., Hahne, K., Emmermann, R., Büsch, W., Gerstenberger, H., Siebel, W., 1999. Evidence for Late Miocene to Recent contamination of arc andesites by crustal melts in the Chilean Andes (25–26°S) and its geodynamic implications. J. South Am. Earth Sci. 12, 135–155. http://dx.doi.org/10.1016/s0895-9811(99)00011-5.

Walker, B.A., Grunder, A.L., Wooden, J.L., 2010. Organization and thermal maturation of long-lived arc systems: evidence from zircons at the Aucanquilcha volcanic cluster, northern Chile. Geology 38, 1007–1010. http://dx.doi.org/10.1130/G31226.1.

Walker, B.A., Klemetti, E.W., Grunder, A.L., Tepley, F.J., Giles, D., 2013. Crystal reaming during the assembly, maturation, and waning of an eleven-million-year crustal magma cycle: thermobarometry of the Aucanquilcha Volcanic Cluster. Contrib. Mineral. Petrol. 165, 663–682. http://dx.doi.org/10.1007/s00410-012-0829-2.

Wood, B.J., Bryndzia, L.T., Johnson, K.E., 1990. Mantle oxidation state and its relationship to tectonic environment and fluid speciation. Science 248, 337–345. http://dx.doi.org/10.1126/science.248.4953.337.

Wright, H.M.N., Folkes, C.B., Cas, R.A.F., Cashman, K.V., 2011. Heterogeneous pumice populations in the 2.08-Ma Cerro Galán Ignimbrite: implications for magma recharge and ascent preceding a large-volume silicic eruption. Bull. Volcanol. 3, 1513–1533. http://dx.doi.org/10.1007/s00445-011-0525-5.

Yuan, X., Sobolev, S.V., Kind, R., 2002. Moho topography in the central Andes and its geodynamic implications. Earth Planet. Sci. Lett. 199, 389–402.